NANO LETTERS

Letter

pubs.acs.org/NanoLett

Nearly Monodisperse Insulator Cs_4PbX_6 (X = Cl, Br, I) Nanocrystals, Their Mixed Halide Compositions, and Their Transformation into $CsPbX_3$ Nanocrystals

Quinten A. Akkerman,[†,‡] Sungwook Park,[†,§] Eros Radicchi,[∥,⊥] Francesca Nunzi,[∥,⊥] Edoardo Mosconi,[∥,#] Filippo De Angelis,[∥,#] Rosaria Brescia,[†] Prachi Rastogi,[†,‡] Mirko Prato,*[,†] and Liberato Manna*[,†]

[†]Nanochemistry Department, Istituto Italiano di Tecnologia, Via Morego 30, 16163 Genova, Italy

[‡]Dipartimento di Chimica e Chimica Industriale, Università degli Studi di Genova, Via Dodecaneso, 31, 16146, Genova, Italy

[§]Department of Physics, Pukyong National University, Busan 608-737, Korea

[∥]Computational Laboratory of Hybrid/Organic Photovoltaics (CLHYO), CNR-ISTM, via Elce di Sotto 8, I-06123 Perugia, Italy

[⊥]Dipartimento di Chimica, Biologia e Biotecnologie, Università degli Studi di Perugia, via Elce di Sotto 8, I-06123 Perugia, Italy

[#]CompuNet, Istituto Italiano di Tecnologia, Via Morego 30, 16163 Genova, Italy

Supporting Information

ABSTRACT: We have developed a colloidal synthesis of nearly monodisperse nanocrystals of pure Cs_4PbX_6 (X = Cl, Br, I) and their mixed halide compositions with sizes ranging from 9 to 37 nm. The optical absorption spectra of these nanocrystals display a sharp, high energy peak due to transitions between states localized in individual PbX_6^{4-} octahedra. These spectral features are insensitive to the size of the particles and in agreement with the features of the corresponding bulk materials. Samples with mixed halide composition exhibit absorption bands that are intermediate in spectral position between those of the pure halide compounds. Furthermore, the absorption bands of intermediate compositions broaden due to the different possible combinations of halide coordination around the Pb^{2+} ions. Both observations are supportive of the fact that the $[PbX_6]^{4-}$ octahedra are electronically decoupled in these systems. Because of the large band gap of Cs_4PbX_6 (>3.2 eV), no excitonic emission in the visible range was observed. The Cs_4PbBr_6 nanocrystals can be converted into green fluorescent $CsPbBr_3$ nanocrystals by their reaction with an excess of $PbBr_2$ with preservation of size and size distributions. The insertion of PbX_2 into Cs_4PbX_6 provides a means of accessing $CsPbX_3$ nanocrystals in a wide variety of sizes, shapes, and compositions, an important aspect for the development of precisely tuned perovskite nanocrystal inks.

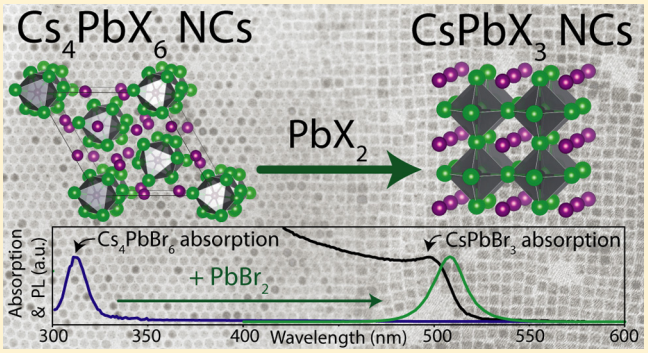

KEYWORDS: *Cs_4PbX_6, nanocrystals, halide perovskites, synthesis, transformations*

Lead halide perovskites (LHPs) recently gained increasing attention due to their optical and electronic properties that have enabled the fabrication of efficient optoelectronic and photovoltaic devices in the time span of only a few years.[1−4] Soon after, the first reports on synthesis methods of high quality LHP nanocrystals (NCs) appeared.[5,6] Nowadays, LHP NCs can be synthesized in a wide range of compositions, sizes, and shapes.[5,7−11] This area of research for what concerns both thin films and NCs was initially focused on the $APbX_3$ perovskite composition (with A being methylammonium or Cs^+ and X being Cl^-, Br^-, I^-), whose structure is characterized by corner sharing $[PbX_6]^{4-}$ octahedra with the A^+ cations filling the voids created by four neighboring PbX_6^{4-} octahedra (Figure 1a).[12,13] Compared to the large band gaps of individual $[PbX_6]^{4-}$ octahedra (≫3.1 eV),[14,15] originating from the splitting of the bonding and antibonding states, the coupling of the octahedra in LHPs leads to materials with much smaller band gaps, spanning the visible region of the spectrum up to the infrared. Recently, layered perovskites too have come into intense scrutiny.[16−20] As an example, the 2D "Ruddlesden−Popper" A_2PbX_4 phase is made of layers of corner-sharing $[PbX_6]^{4-}$ octahedra alternating with layers of bulky cations. This is often realized by using a mixture of smaller and larger (for example butylammonium) monovalent cations.[16−18] In these 2D structures, like the one mentioned above, the exciton can no longer propagate in all dimensions and instead it is confined in the two-dimensional PbX_6^{4-} layers, resulting in larger band gaps compared to the ABX_3 phase. As an example,

Received: December 19, 2016
Revised: February 1, 2017
Published: February 14, 2017

DOI: 10.1021/acs.nanolett.6b05262
Nano Lett. 2017, 17, 1924−1930

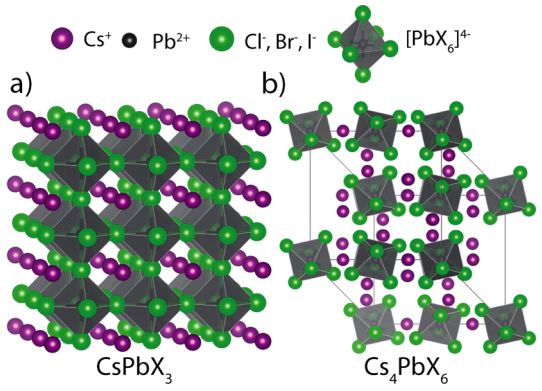

Figure 1. Structural models of (a) 3D cubic $CsPbX_3$ and (b) 0D hexagonal Cs_4PbX_6 perovskites with X = Cl, Br, I.

$(ODA)_2PbBr_4$ (with ODA = octadecylammonium) has a 3.1 eV (400 nm) band gap, whereas $CsPbBr_3$ has a 2.36 eV (525 nm) band gap.[21] Finally, in the A_4PbX_6 structure (A = Rb^+, Cs^+), the PbX_6^{4-} octahedra are completely decoupled in all dimensions (Figure 1b),[22−26] and the optical properties of such crystals closely resemble those of individual $[PbX_6]^{4-}$ clusters that have been observed experimentally in halide salts doped with Pb^{2+} ions.[14,15] This results in insulator band gaps (Cs_4PbCl_6 = 4.37 eV, Cs_4PbBr_6 = 3.95 eV, and Cs_4PbI_6 = 3.38 eV),[23−27] and the A_4PbX_6 phase is thus often referred to as a zero-dimensional (0D) perovskite. While the 3D and 2D phases of LHPs are widely studied and well understood, 0D perovskites are comparatively less explored with only very recent works revisiting the optical properties of Cs_4PbBr_6 powders and single crystals.[28−30]

Here, we report a fast and simple ambient synthesis method for Cs_4PbX_6 (X = Cl, Br, I) NCs, by working under Cs^+ rich reaction conditions compared to the traditional $CsPbX_3$ NC synthesis.[5] The NCs are nearly monodisperse and their size can be tuned from 9 to 37 nm. They have large band gaps and their optical absorption spectra are characterized by strong and narrow bands, independent of the size of the NCs. Furthermore, NCs with mixed halide composition (either Cl/Br or Br/I) can be prepared either by direct synthesis or by mixing presynthesized NCs with different halide compositions, via interparticle anion exchange. The mixed halide NCs have optical absorption bands that are at intermediate spectral positions compared to their pure halide counterparts and much broader than in the pure halides, indicating that they contain various populations of $[PbX_6]^{4-}$ octahedra with different combinations of halide ions, as also supported by density functional theory (DFT) calculations. Finally, the Cs_4PbBr_6 NCs can be transformed into strongly fluorescent $CsPbBr_3$ NCs via an insertion reaction with additional $PbBr_2$. Not only does this allow for the synthesis of large $CsPbBr_3$ NCs with high level of control over the size (from 9 up to 37 nm) but it also opens up a reliable postsynthesis method for the fabrication of novel NC compositions.

The Cs_4PbBr_6 NCs were prepared by modifying the traditional synthesis approach for $CsPbBr_3$ NCs[5] by using an excess of Cs-oleate and lowering the reaction temperature, as detailed in the Supporting Information (SI). As seen from the transmission electron microscopy (TEM) images of Figure 2a−d and Figure S1, this resulted in nearly monodisperse Cs_4PbBr_6 NCs ranging from 9 to 37 nm. The monodispersity of the Cs_4PbBr_6 NCs was such that by TEM we could easily identify large area monolayer self-assemblies and 3D supercrystals (see also Figure S2). The size of the NCs could be controlled by tuning the reaction temperature and the time. High-resolution TEM (HRTEM, Figure 2e) and X-ray diffraction (XRD, see Figures 2f and S3a) indicated that all the NCs have the hexagonal Cs_4PbBr_6 phase and no $CsPbBr_3$ phase was present. All the Cs_4PbBr_6 NC dispersions were colorless, with the smaller NC dispersions being completely transparent and the larger ones (from 17 nm and bigger) being turbid. The samples had a strong and narrow optical absorption band at 314 nm,

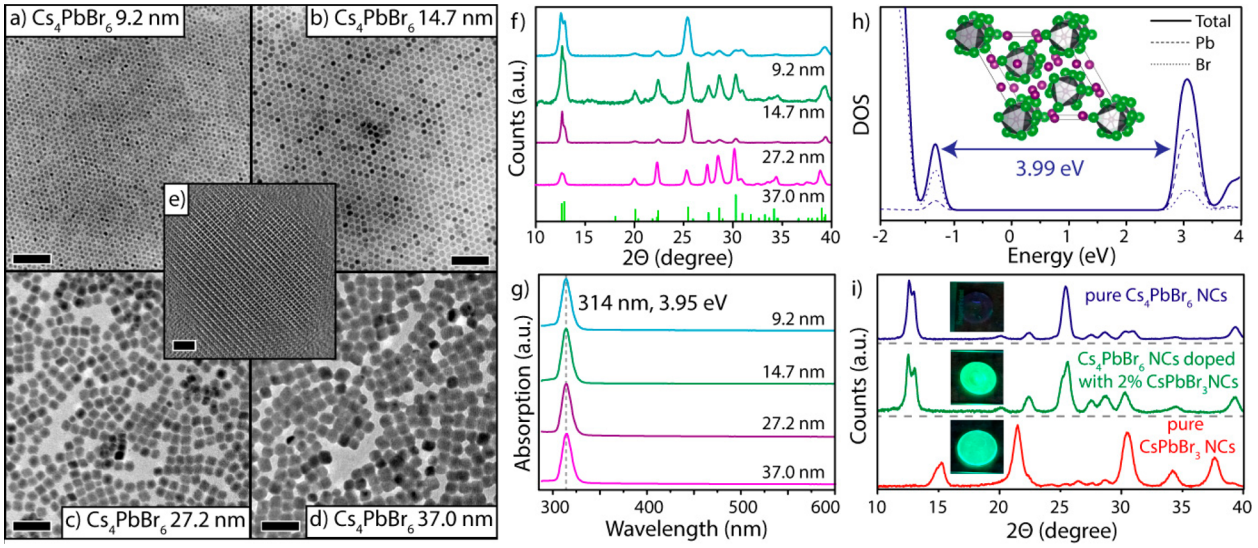

Figure 2. TEM images of (a) 9.2, (b) 14.7, (c) 27.2, and (d) 37.0 nm Cs_4PbBr_6 NCs. (e) HRTEM image of a Cs_4PbBr_6 NC. (f) XRD patterns of different sized Cs_4PbBr_6 NCs matching with the Cs_4PbBr_6 reference pattern (98-002-5124). (g) Optical absorption spectra of different sized Cs_4PbBr_6 NCs, characterized by a strong absorption band at 314 nm, independent of the NC size. (h) DFT density of states calculation of Cs_4PbBr_6 confirming the large band gap of 3.99 eV. (i) Comparison of pure Cs_4PbBr_6 NC film, pure $CsPbBr_3$ NC film and a Cs_4PbBr_6 NC film intentionally doped with 2% $CsPbBr_3$ NCs. The latter sample has a PL that is typical of $CsPbBr_3$, but its diffraction pattern can be indexed with the Cs_4PbBr_6 phase alone. Scale bars are 100 nm in all TEM images and 2 nm in the HRTEM image.

DOI: 10.1021/acs.nanolett.6b05262
Nano Lett. 2017, 17, 1924−1930

regardless of NC size (Figures 2g and S3b), matching with previous reports on bulk Cs_4PbBr_6 powders and films.[26,27] This supports the fact that the $[PbX_6]^{4-}$ octahedra in the Cs_4PbBr_6 NCs are completely decoupled, and thus the size of the NCs does not have any remarkable effect on the band structure. In comparison, $CsPbBr_3$ NCs still exhibit quantum confinement effects for sizes around 8−9 nm and beyond (this point is further discussed in later sections of this work).[5] No strong photoluminescence (PL) was observed from any of the Cs_4PbBr_6 NCs. This matches with previous reports on Cs_4PbBr_6 films and crystals, in which the excitonic PL decayed significantly at temperatures above 100 K.[27] All samples of Cs_4PbBr_6 NCs, as well as the corresponding Cl and I compositions (discussed later), prepared by us did exhibit a weak PL band around 380 nm, but this was independent of the halide composition and was therefore assigned to ligands emission because a similar emission was observed from a mixture of the surfactants used for their syntheses.

To confirm the wide band gap of Cs_4PbBr_6, we carried out DFT calculations within periodic boundary conditions on the experimentally reported structure of Cs_4PbBr_6. The calculated density of states is displayed in Figure 2h (see also Figure S4 that compares the density of states of Cs_4PbBr_6 with that of $CsPbBr_3$). The Br-based valence band and the Pb-based conduction bands are separated by a band gap of 3.99 eV, which is in close agreement with the band gap value of 3.95 eV by Nikl et al. for Cs_4PbBr_6 films[27] (the same value of 3.95 eV was found also by us on the Cs_4PbBr_6 NCs of this work). Interestingly, DFT calculations evidenced almost no band dispersion within 30 meV or less across different k-points, suggesting closely to uncoupled $PbBr_6$ octahedra. Despite Cs_4PbBr_6 being a large band gap material, several groups have reported strong, green luminescent from Cs_4PbBr_6 powders, single-crystals, and NCs.[28−30] Our opinion on these works is that the green PL in Cs_4PbBr_6 originates rather from minor nanoscale $CsPbBr_3$ impurities encapsulated in the Cs_4PbBr_6 bulk matrix. Because $CsPbBr_3$ NCs can have very high PL quantum yields (PLQYs), up to 95%, only a very small fraction of them can be enough to result in a green, $CsPbBr_3$-like emission, disguised as deriving from the whole sample, even if apparently no trace of $CsPbBr_3$ can be found by X-ray diffraction analysis. Doubts on the fact that such green emission comes from Cs_4PbBr_6 have also been expressed in a recent review article on halide perovskite nanosystems.[31] Also, even Nikl et al. in their 1999 work on Cs_4PbBr_6 films observed an emission peak at 545 nm, which they ascribed to an impurity $CsPbBr_3$-like phase.[27]

To prove our point, we added a small amount of $CsPbBr_3$ NCs to a solution of Cs_4PbBr_6 NCs, such that the molar ratio of $CsPbBr_3$ NCs to Cs_4PbBr_6 was only 2%, as determined by elemental analysis on Pb via inductively coupled plasma optical emission spectroscopy. Solutions of pure Cs_4PbBr_6 NCs, pure $CsPbBr_3$ NCs, and of Cs_4PbBr_6 NCs "doped" with 2% $CsPbBr_3$ NCs were deposited on a substrate, dried, and their PL and XRD patterns were recorded. The relevant data are reported in Figure 2i. The pure Cs_4PbBr_6 NC film exhibited no green luminescence, similar to the Cs_4PbBr_6 NCs in solution. The film doped with 2% $CsPbBr_3$ exhibited instead a strong green PL, similar to that of the film of pure $CsPbBr_3$ NCs, even though from its XRD pattern one would conclude that this sample was made of pure Cs_4PbBr_6 phase. Overall, we conclude that to date it has been difficult to prepare optically pure Cs_4PbBr_6, neither in bulk form nor as colloidal particles, and we see no reason why this material, in its pure form, should be green emitting.

Next to the Cs_4PbBr_6 NCs, we could synthesize nearly monodisperse Cs_4PbCl_6 (17.0 ± 1.4 nm) and Cs_4PbI_6 NCs (10.0 ± 0.8 nm) by simply replacing $PbBr_2$ with $PbCl_2$ or PbI_2, respectively (Figures 3a,b and S5). Both HRTEM (inset Figure 3c,d, respectively) and XRD (Figures 3e and S6) indicate that the Cs_4PbCl_6 and Cs_4PbI_6 NCs are crystalline and match with the reported pure Cs_4PbX_6 phases. As in the case of Cs_4PbBr_6, the Cs_4PbCl_6 and Cs_4PbI_6 NCs have wide band gaps (respectively 284 and 367 nm as shown in Figure 3f).[23,24,26] All Cs_4PbX_6 NCs, including the Cs_4PbI_6 NCs, remained stable under ambient conditions over the course of at least one month without any sign of degradation (Figure S7). Although all Cs_4PbX_6 NCs could simply be separated by centrifugation, due to the lower solubility of the Cs_4PbX_6 phase compared to the $CsPbX_3$ phase,[32] they could be washed several times with polar solvents like acetonitrile and isopropanol without being dissolved (Figure S8). The Cs_4PbI_6 NCs still remained susceptible toward polar solvents and were readily dissolved in isopropanol and acetonitrile, as NC dispersions quickly turned dark red/brown due to the formation of solvated I^- ions.

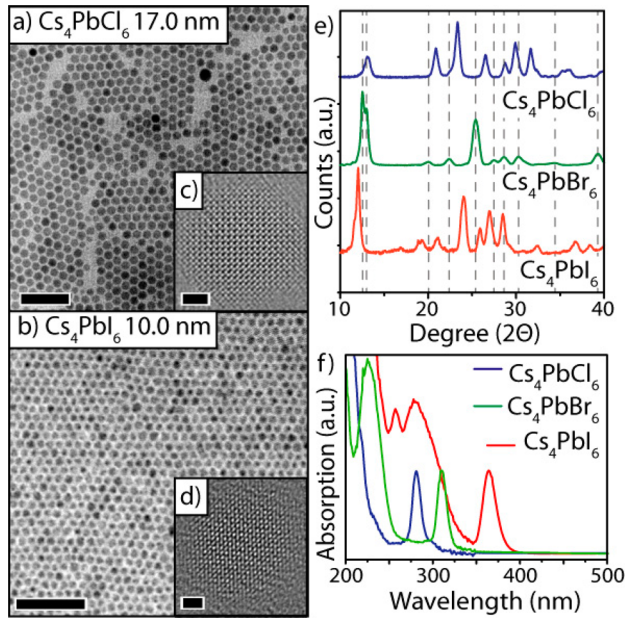

Figure 3. TEM images of (a) Cs_4PbCl_6 and (b) Cs_4PbI_6 NCs with HRTEM images in their respective insets (c,d). (e) XRD patterns of pure Cs_4PbX_6 NCs showing evident shifts toward larger unit cells when going from Cl to Br and then to I. (f) Absorption spectra of pure Cs_4PbX_6 NCs. Scale bars are 100 nm in all TEM images and 2 nm in all the HRTEM images.

Similarly to the amply reported cases of $CsPbX_3$,[5,33,34] Cs_4PbX_6 NCs as well can form stable mixed halide compositions, as shown in Figure 4. For example, both $Cs_4Pb(Br/Cl)_6$ (16.5 + 3.0 nm) and $Cs_4Pb(Br/I)_6$ (13.6 + 3.4 nm) NCs were prepared by mixing 14.7 nm Cs_4PbBr_6 NCs with 10.0 nm Cs_4PbCl_6 NCs or 17.0 nm Cs_4PbI_6 NCs (Figure 4a,b, respectively). With preservation of size distributions, the NCs underwent interparticle halide exchange, resulting in the mixed $Cs_4Pb(Br/X)_6$ phase.[34] The formation of the mixed phases could be inferred from the XRD patterns, as shown in Figure 4c. After the exchange, the NCs had lattice parameters

DOI: 10.1021/acs.nanolett.6b05262
Nano Lett. 2017, 17, 1924−1930

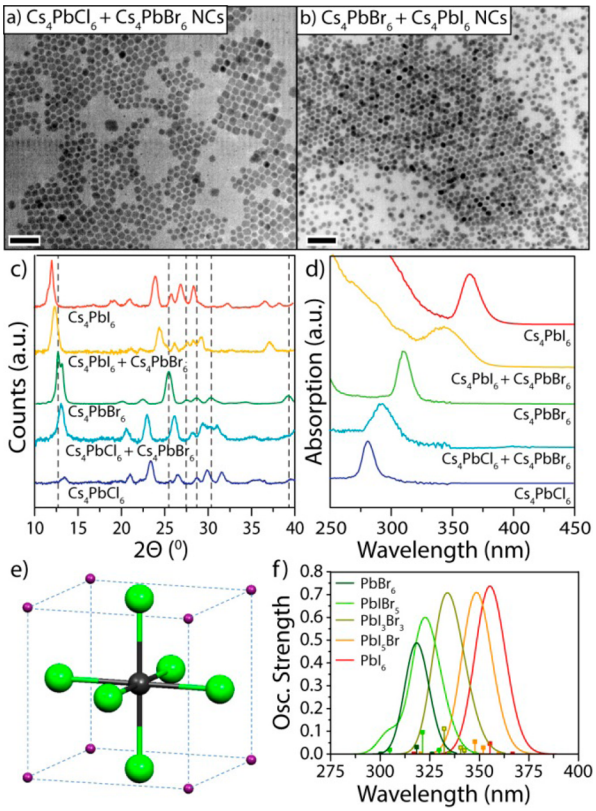

Figure 4. TEM images of NCs obtained after interparticle anion exchange of Cs_4PbBr_6 NCs with (a) Cs_4PbCl_6 and (b) Cs_4PbI_6. Scale bars are 100 nm in both images. (c) XRD patterns confirm intermediate crystal phase after exchange. (d) Optical absorption spectra recorded on pristine and mixed NCs with intermediate, broadened absorptions. (e) Sketch of the PbX_6 model used for the calculations with point charges at the cubic sites. (f) Simulated absorption spectra of charge-compensated PbI_6, $PbBr_6$, and intermediate compositions. The calculated TDDFT excitation energies and oscillator strengths have been convoluted by Gaussian functions with a σ = 0.075 eV.

that were intermediate between the starting pure halide NCs, and no diffraction peaks could be observed for the pure starting phases. In the optical absorption spectra, intermediate band gaps of 305 nm for the $Cs_4Pb(Br/Cl)_6$ NCs and 343 nm for the $Cs_4Pb(Br/I)_6$ NCs were observed (Figure 4d). Mixed $Cs_4Pb(Br/Cl)_6$ and $Cs_4Pb(Br/I)_6$ NCs could also be obtained by directly starting with mixed PbX_2 precursors (by partially replacing $PbBr_2$ with $PbCl_2$ or PbI_2 prior to the synthesis), as shown in Figure S9. The directly obtained mixed Cs_4PbX_6 NCs also exhibited properties intermediate to their respective pure phases.

The Cs_4PbX_6 NCs with mixed halide composition shown here had a significantly broader absorption band compared to the pure Cs_4PbX_6 NCs (Figures 4d and S9d). This is markedly different from the case of $CsPbX_3$ NCs with mixed halide composition reported in previous works (which could be prepared by partial anion exchange as well), for which the absorption spectrum (and the PL spectrum) remained narrow.[33,34] Focusing, for example, on the Br/I mixed composition, it can be stated that in the $CsPbX_3$ 3D perovskite structure all the $[PbBr_xI_{6-x}]^{4-}$ octahedra are electronically coupled and such coupling dictates the overall band structure. In the Cs_4PbX_6 case, as already stated, the octahedra are no longer electronically coupled and the absorption is due to a collection of electronic transitions within the single $[PbX_6]^{4-}$ clusters. Therefore, the overall optical absorption from $Cs_4Pb(Br/I)_6$ can be considered as a summation of the independent, weighted contributions from the different populations of octahedra present in the sample. Note that each population differs from the others by the distinct numbers of I^- and Br^- ions (totaling 6) coordinating the Pb^{2+} ion, that is, $[PbBr_xI_{6-x}]^{4-}$ with x = 0, 1, 2, up to 6, and by the specific arrangement of the anions at the six corners of the complex with Pb^{2+}. Consequently, each population will be characterized by its own electronic transitions. The broadening in the absorption is thus explained by the different spectral positions, detailed features, and relative contributions of each of these populations within a single NC.

The optical properties of the pure and mixed-halide Cs_4PbX_6 were also investigated by means of hybrid time-dependent DFT (TDDFT) calculations including spin−orbit coupling (SOC),[35] as implemented in the ADF package;[36] see SI for further details. The TDDFT calculations were carried out on a simplified model made by a single PbX_xY_{6-x} cluster (X, Y = I, Br or Br, Cl) in cubic symmetry (total charge −4), where the Cs cations are replaced by 8 point charges, each of +0.5e, placed at the corner cubic sites, equivalent to an overall neutralizing charge of +4, see Figure 4e. The accuracy of the model has been validated through comparative calculations on both the Cs_4PbBr_6 cluster extracted from the XRD structure and the charge-compensated $PbBr_6^{4-}$ anion, delivering a highest occupied molecular orbital−lowest unoccupied molecular orbital (HOMO−LUMO) gap difference within 0.2 eV; this simplified model is also justified in light of the vanishingly small band dispersion found by periodic DFT calculations. The employed model allowed us to effectively capture the optical transition features of individual NCs, beyond a simple single particle approximation. Notably, the effect of SOC, established in 3D and 2D LHPs,[37] is found to be relevant also in the case of 0D NCs, as it introduces a decrease of the HOMO−LUMO gap and a red-shift of the calculated absorption spectra by as much as 0.5 eV. This is due to both the stabilization of the unoccupied Pb 6p states (~0.3 eV) and the destabilization of the occupied halide p states (~0.2 eV for the X = I case).

The calculated absorption spectra for charge compensated PbI_6, $PbBr_6$, and for a range of I−Br intermediate compositions are reported in Figure 4f. The calculations almost quantitatively reproduce the absorption spectra of the pure Cs_4PbX_6 NCs for X = I and Br (355 and 319 nm against experimental values for the corresponding NCs of 367 and 314 nm, respectively). The mixed I/Br compositions show an almost monotonic variation of the absorption maxima across the explored compositional range, see Figure 4f. Notably, for the intermediate PbI_3Br_3 system we calculate an absorption maximum at 334 nm, which is in agreement with the experimental maximum of 343 nm for the mixed halide system. Also, the broadening of the experimental spectrum for the mixed halide system is compatible with a full range of intermediate compositions, which we calculated with a spread of about ±0.15 eV from the median PbI_3Br_3 system. We also ran some preliminary calculations for the X = Cl case (data not shown). In that case, however, the optical transitions are underestimated by our approach, providing an absorption maximum of 316 nm against an experimental value of 284 nm for Cs_4PbCl_6. This is likely due to the unbalanced description of the halide series by (hybrid) DFT, which can be corrected by GW calculations.[38]

DOI: 10.1021/acs.nanolett.6b05262
Nano Lett. 2017, 17, 1924−1930

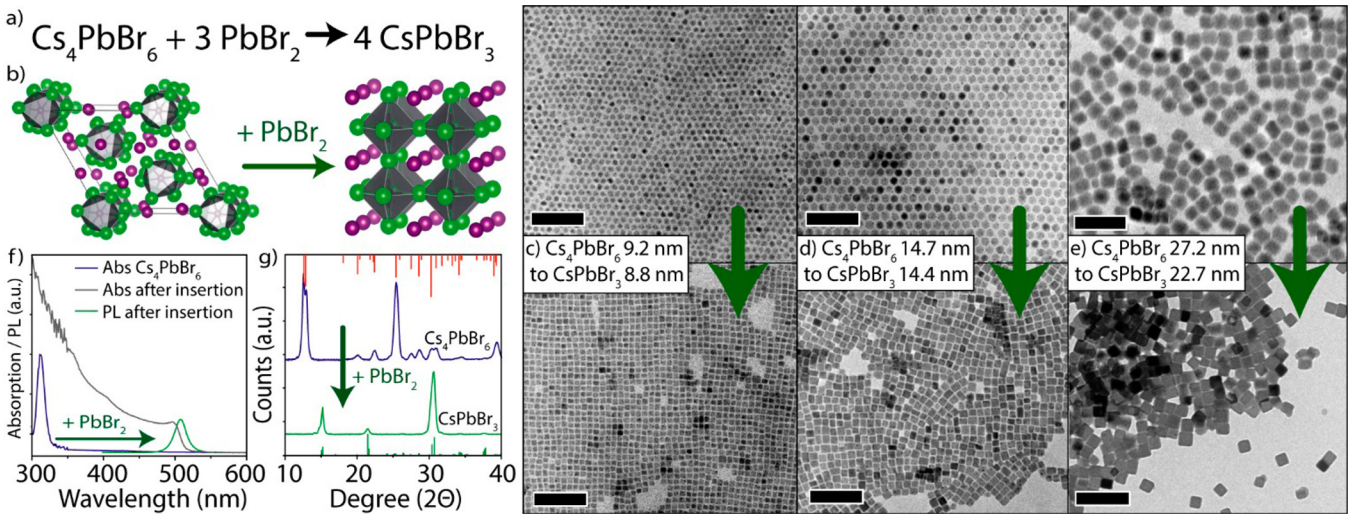

Figure 5. (a) Reaction of Cs_4PbBr_6 with $PbBr_2$, forming $CsPbBr_3$. (b) Phase transformation of the hexagonal Cs_4PbBr_6 phase to the cubic $CsPbBr_3$ phase after insertion of additional $PbBr_2$. (c–e) TEM images of different-sized Cs_4PbBr_6 NCs before and after their transformation into $CsPbBr_3$, indicating the preservation of size but transformation of the hexagonal shape to a cubic shape. (f) Optical absorption and PL of pristine Cs_4PbBr_6 NCs and of the same sample after the insertion reaction, highlighting the large shift of the band gap, the disappearance of the strong Cs_4PbBr_6 absorption feature and the appearance of a strong green PL after the transformation. (g) XRD patterns before and after the insertion reaction, confirming the rearrangement of the crystal lattice from hexagonal Cs_4PbBr_6 to cubic $CsPbBr_3$. Scale bars are 100 nm in all TEM images. XRD references patterns are 98-010-9295 for $CsPbBr_3$ and 98-002-5124 for Cs_4PbBr_6.

The hexagonal phase Cs_4PbBr_6 NCs reported in this work have high band gaps and therefore are essentially insulators. Also, the lack of strong, excitonic fluorescence prevents their use in applications such as active materials in scintillators. On the other hand, we found that they could be transformed to $CsPbBr_3$ NCs by a postsynthesis insertion reaction with $PbBr_2$ as shown in Figure 5a,b. Here, the Cs_4PbBr_6 NCs were exposed to a solution of $PbBr_2$ dissolved in oleylamine, oleic acid, and toluene. As shown in Figures 5c,d and S10, this results in the reshaping of the NCs from a spherical/hexagonal shape to cubic NCs. Although the NCs underwent a shape transformation, the overall size was basically preserved. It is important to note that the NCs did not undergo any transformation in the absence of $PbBr_2$ under the same reaction conditions (as shown in Figure S11). Because of the high monodispersity of the starting Cs_4PbBr_6 NCs, this resulted in close to monodisperse cubic $CsPbBr_3$ NCs within a wide range of sizes (8.8–34.0 nm, see also Figure S10). These data strongly support the idea that the Cs_4PbBr_6 NCs underwent a transformation to $CsPbBr_3$ NCs and exclude the possibility that they were dissolved and that new $CsPbBr_3$ NCs were nucleated. In this latter scenario, the sizes of the starting Cs_4PbBr_6 NCs and those of the final $CsPbBr_3$ NCs would be uncorrelated, which is in contrast with our observations. With this approach, we could even synthesize large (>15 nm) and yet nearly monodisperse $CsPbBr_3$ NCs, which currently remains a challenge in conventional $CsPbBr_3$ NC synthesis methods.[39,40]

The formation of the $CsPbBr_3$ phase resulted in a large shift of the absorption band (from 314 to 510 nm) and the emergence of a strong green PL in the 511–522 nm range, depending on the size of the pristine NCs (Figure S12a). Furthermore, no absorption feature from the pristine NCs was observed (Figure S12b). Although this implies that the transformation is complete, the PLQYs only ranged from ~26% for the smallest (~9 nm) NCs to 2.4% for the largest (34 nm) NCs. The smallest $CsPbBr_3$ NCs still exhibited a weak confinement compared to the bulk-like emission of the larger NCs (Figure S12a). Yet, for such small NCs the PLQY was lower than that reported from NCs of similar size and prepared by direct synthesis. Upon increasing the reaction temperature (from 80 to 130 °C and a fourfold amount of $PbBr_2$), the PLQY for the smallest NCs could be increased from 26 to 47%. For now, these lower PLQY values (compared to those of NCs prepared by direct synthesis) indicate that the transformation from the hexagonal Cs_4PbBr_6 to the cubic $CsPbBr_3$ phase may entail the formation of structural defects acting as trap states, especially at lower temperatures and lower $PbBr_2$ concentrations, and suggest that such two-step synthesis would require further tuning. Additional optimizations of this conversion reaction are likely to push the PLQY to values close to those of directly synthesized $CsPbBr_3$ NCs. The transformation of the Cs_4PbBr_6 NCs was also confirmed by XRD, as reported in Figures 5g and S12c. Here, the diffraction pattern from the transformed $CsPbBr_3$ NCs matched with that of the cubic/orthorhombic phase with no measurable diffractions from the pristine NCs. The Cs_4PbCl_6 NCs too could be converted into $CsPbCl_3$ NCs by the addition of $PbCl_2$. Figure S13 reports the optical data referred to the $Cs_4PbCl_6 \rightarrow CsPbCl_3$ transformation. In the $Cs_4PbI_6 \rightarrow CsPbI_3$ case, the $CsPbI_3$ NCs were quickly degraded and their PL was rapidly quenched, which is expected due to the well-known intrinsic instability of the pure $CsPbI_3$ phase.[41,42] These reactions were not further investigated and will require additional work.

In conclusion, we have reported here a method for preparing monodisperse NCs of Cs_4PbX_6 (X = Cl, Br, I) and of their mixed halide compositions. Contrary to recent reports, we found no evidence of green emission from these 0D NCs, which we believe originated from the presence of $CsPbBr_3$ impurities in those works. The Cs_4PbBr_6 NCs were used here as a starting point to synthesize monodisperse $CsPbBr_3$ NCs by further reaction with $PbBr_2$. This transformation is yet another proof of the versatility of the perovskite crystal structure, which allows for extreme reorganization of the lattice. In the NC case, this enables preservation of NC size and crystallinity. One

DOI: 10.1021/acs.nanolett.6b05262
Nano Lett. 2017, 17, 1924–1930

important development in this direction will be in understanding the detailed structural intermediates of the transformation and the use of this type of "insertion reaction" in other classes of NCs.

■ ASSOCIATED CONTENT

Supporting Information

The Supporting Information is available free of charge on the ACS Publications website at DOI: 10.1021/acs.nanolett.6b05262.

Experimental and computational details; additional TEM images, absorption spectra and diffraction patterns for different sizes Cs_4PbBr_6 NCs and the $CsPbBr_3$ NCs; additional details on diffraction patterns for Cs_4PbCl_6 and Cs_4PbI_6 NCs. TEM, XRD, and absorption spectra for mixed halide Cs_4PbX_6 NCs (PDF)

■ AUTHOR INFORMATION

Corresponding Authors

*E-mail: mirko.prato@iit.it.

*E-mail: liberato.manna@iit.it.

ORCID

Filippo De Angelis: 0000-0003-3833-1975

Mirko Prato: 0000-0002-2188-8059

Liberato Manna: 0000-0003-4386-7985

Author Contributions

Q.A.A. and S.P. contributed equally to this work.

Notes

The authors declare no competing financial interest.

■ ACKNOWLEDGMENTS

The research leading to these results has received funding from the European Union seventh Framework Programme under Grant Agreement No. 614897 (ERC Consolidator Grant "TRANS-NANO") and framework programme for research and Innovation Horizon 2020 (2014-2020) under the Marie Skłodowska-Curie Grant Agreement COMPASS No. 691185, and from the Basic Science Research Program through the National Research Foundation of Korea(NRF) funded by the Ministry of Education(NRF-2014R1A1A2009367).

■ REFERENCES

(1) Saliba, M.; Orlandi, S.; Matsui, T.; Aghazada, S.; Cavazzini, M.; Correa-Baena, J.-P.; Gao, P.; Scopelliti, R.; Mosconi, E.; Dahmen, K.-H.; De Angelis, F.; Abate, A.; Hagfeldt, A.; Pozzi, G.; Graetzel, M.; Nazeeruddin, M. K. *Nat. Energy* **2016**, *1*, 15017.

(2) Saliba, M.; Matsui, T.; Seo, J.-Y.; Domanski, K.; Correa-Baena, J.-P.; Nazeeruddin, M. K.; Zakeeruddin, S. M.; Tress, W.; Abate, A.; Hagfeldt, A.; Gratzel, M. *Energy Environ. Sci.* **2016**, *9*, 1989−1997.

(3) Yang, W. S.; Noh, J. H.; Jeon, N. J.; Kim, Y. C.; Ryu, S.; Seo, J.; Seok, S. I. *Science* **2015**, *348*, 1234−1237.

(4) Cho, H.; Jeong, S.-H.; Park, M.-H.; Kim, Y.-H.; Wolf, C.; Lee, C.-L.; Heo, J. H.; Sadhanala, A.; Myoung, N.; Yoo, S.; Im, S. H.; Friend, R. H.; Lee, T.-W. *Science* **2015**, *350*, 1222−1225.

(5) Protesescu, L.; Yakunin, S.; Bodnarchuk, M. I.; Krieg, F.; Caputo, R.; Hendon, C. H.; Yang, R. X.; Walsh, A.; Kovalenko, M. V. *Nano Lett.* **2015**, *15*, 3692−3696.

(6) Schmidt, L. C.; Pertegás, A.; González-Carrero, S.; Malinkiewicz, O.; Agouram, S.; Mínguez Espallargas, G.; Bolink, H. J.; Galian, R. E.; Pérez-Prieto, J. *J. Am. Chem. Soc.* **2014**, *136*, 850−853.

(7) Akkerman, Q. A.; Motti, S. G.; Srimath Kandada, A. R.; Mosconi, E.; D'Innocenzo, V.; Bertoni, G.; Marras, S.; Kamino, B. A.; Miranda, L.; De Angelis, F.; Petrozza, A.; Prato, M.; Manna, L. *J. Am. Chem. Soc.* **2016**, *138*, 1010−1016.

(8) Zhu, F.; Men, L.; Guo, Y.; Zhu, Q.; Bhattacharjee, U.; Goodwin, P. M.; Petrich, J. W.; Smith, E. A.; Vela, J. *ACS Nano* **2015**, *9*, 2948−2959.

(9) Vybornyi, O.; Yakunin, S.; Kovalenko, M. V. *Nanoscale* **2016**, *8*, 6278−6283.

(10) Protesescu, L.; Yakunin, S.; Bodnarchuk, M. I.; Bertolotti, F.; Masciocchi, N.; Guagliardi, A.; Kovalenko, M. V. *J. Am. Chem. Soc.* **2016**, *138*, 14202−14205.

(11) Liu, W.; Lin, Q.; Li, H.; Wu, K.; Robel, I.; Pietryga, J. M.; Klimov, V. I. *J. Am. Chem. Soc.* **2016**, *138*, 14954−14961.

(12) Boix, P. P.; Agarwala, S.; Koh, T. M.; Mathews, N.; Mhaisalkar, S. G. *J. Phys. Chem. Lett.* **2015**, *6*, 898−907.

(13) Walsh, A. *J. Phys. Chem. C* **2015**, *119*, 5755−5760.

(14) Bohun, A.; Dolejší, J.; Barta, Č. *Czech. J. Phys.* **1970**, *20*, 803−807.

(15) Polak, K.; Nikl, M.; Mihokova, E. *J. Lumin.* **1992**, *54*, 189−196.

(16) Calabrese, J.; Jones, N. L.; Harlow, R. L.; Herron, N.; Thorn, D. L.; Wang, Y. *J. Am. Chem. Soc.* **1991**, *113*, 2328−2330.

(17) Mitzi, D. B. *Chem. Mater.* **1996**, *8*, 791−800.

(18) Quan, L. N.; Yuan, M.; Comin, R.; Voznyy, O.; Beauregard, E. M.; Hoogland, S.; Buin, A.; Kirmani, A. R.; Zhao, K.; Amassian, A.; Kim, D. H.; Sargent, E. H. *J. Am. Chem. Soc.* **2016**, *138*, 2649−2655.

(19) Huan, T. D.; Tuoc, V. N.; Minh, N. V. *Phys. Rev. B: Condens. Matter Mater. Phys.* **2016**, *93*, 094105.

(20) Pedesseau, L.; Sapori, D.; Traore, B.; Robles, R.; Fang, H.-H.; Loi, M. A.; Tsai, H.; Nie, W.; Blancon, J.-C.; Neukirch, A.; Tretiak, S.; Mohite, A. D.; Katan, C.; Even, J.; Kepenekian, M. *ACS Nano* **2016**, *10*, 9776−9786.

(21) Gonzalez-Carrero, S.; Espallargas, G. M.; Galian, R. E.; Perez-Prieto, J. *J. Mater. Chem. A* **2015**, *3*, 14039−14045.

(22) Moller, C. K. *Nature* **1958**, *182*, 1436−1436.

(23) Kondo, S.; Amaya, K.; Higuchi, S.; Saito, T.; Asada, H.; Ishikane, M. *Solid State Commun.* **2001**, *120*, 141−144.

(24) Nikl, M.; Mihokova, E.; Nitsch, K. *Solid State Commun.* **1992**, *84*, 1089−1092.

(25) Kondo, S.; Masaki, A.; Saito, T.; Asada, H. *Solid State Commun.* **2002**, *124*, 211−214.

(26) Kondo, S.; Amaya, K.; Saito, T. *J. Phys.: Condens. Matter* **2002**, *14*, 2093.

(27) Nikl, M.; Mihokova, E.; Nitsch, K.; Somma, F.; Giampaolo, C.; Pazzi, G. P.; Fabeni, P.; Zazubovich, S. *Chem. Phys. Lett.* **1999**, *306*, 280−284.

(28) Saidaminov, M. I.; Almutlaq, J.; Sarmah, S.; Dursun, I.; Zhumekenov, A. A.; Begum, R.; Pan, J.; Cho, N.; Mohammed, O. F.; Bakr, O. M. *ACS Energy Lett.* **2016**, *1*, 840−845.

(29) Chen, D.; Wan, Z.; Chen, X.; Yuan, Y.; Zhong, J. *J. Mater. Chem. C* **2016**, *4*, 10646−10653.

(30) Cha, J.-H.; Han, J. H.; Yin, W.; Park, C.; Park, Y.; Ahn, T. K.; Cho, J. H.; Jung, D.-Y. *J. Phys. Chem. Lett.* **2017**, *8*, 565−570.

(31) Li, X.; Cao, F.; Yu, D.; Chen, J.; Sun, Z.; Shen, Y.; Zhu, Y.; Wang, L.; Wei, Y.; Wu, Y.; Zeng, H. *Small* **2017**, 1603996.

(32) Dirin, D. N.; Cherniukh, I.; Yakunin, S.; Shynkarenko, Y.; Kovalenko, M. V. *Chem. Mater.* **2016**, *28*, 8470−8474.

(33) Nedelcu, G.; Protesescu, L.; Yakunin, S.; Bodnarchuk, M. I.; Grotevent, M. J.; Kovalenko, M. V. *Nano Lett.* **2015**, *15*, 5635−5640.

(34) Akkerman, Q. A.; D'Innocenzo, V.; Accornero, S.; Scarpellini, A.; Petrozza, A.; Prato, M.; Manna, L. *J. Am. Chem. Soc.* **2015**, *137*, 10276−10281.

(35) Wang, F.; Ziegler, T. *J. Chem. Phys.* **2005**, *123*, 194102.

(36) te Velde, G.; Bickelhaupt, F. M.; Baerends, E. J.; Fonseca Guerra, C.; van Gisbergen, S. J. A.; Snijders, J. G.; Ziegler, T. *J. Comput. Chem.* **2001**, *22*, 931−967.

(37) Even, J.; Pedesseau, L.; Jancu, J.-M.; Katan, C. *J. Phys. Chem. Lett.* **2013**, *4*, 2999−3005.

(38) Mosconi, E.; Umari, P.; De Angelis, F. *Phys. Chem. Chem. Phys.* **2016**, *18*, 27158−27164.

DOI: 10.1021/acs.nanolett.6b05262
Nano Lett. 2017, 17, 1924−1930

(39) Koolyk, M.; Amgar, D.; Aharon, S.; Etgar, L. *Nanoscale* **2016**, *8*, 6403−6409.
(40) Pan, A.; He, B.; Fan, X.; Liu, Z.; Urban, J. J.; Alivisatos, A. P.; He, L.; Liu, Y. *ACS Nano* **2016**, *10*, 7943−7954.
(41) Luo, P.; Xia, W.; Zhou, S.; Sun, L.; Cheng, J.; Xu, C.; Lu, Y. *J. Phys. Chem. Lett.* **2016**, *7*, 3603−3608.
(42) Eperon, G. E.; Paterno, G. M.; Sutton, R. J.; Zampetti, A.; Haghighirad, A. A.; Cacialli, F.; Snaith, H. J. *J. Mater. Chem. A* **2015**, *3*, 19688−19695.

DOI: 10.1021/acs.nanolett.6b05262
Nano Lett. 2017, 17, 1924−1930